Dalton Transactions

PAPER

View Article Online
View Journal

Cite this: DOI: 10.1039/c4dt02461c

Photo-induced reduction of CO_2 using a magnetically separable Ru-CoPc@TiO_2@SiO_2@Fe_3O_4 catalyst under visible light irradiation†

Pawan Kumar,[a] R. K. Chauhan,[b] Bir Sain[a] and Suman L. Jain*[a]

Received 14th August 2014,
Accepted 19th January 2015

DOI: 10.1039/c4dt02461c

www.rsc.org/dalton

An efficient photo-induced reduction of CO_2 using magnetically separable Ru-CoPc@TiO_2@SiO_2@Fe_3O_4 as a heterogeneous catalyst in which CoPc and Ru(bpy)$_2$phene complexes were attached to a solid support *via* covalent attachment under visible light is described. The as-synthesized catalyst was characterized by a series of techniques including FTIR, UV-Vis, XRD, SEM, TEM, *etc*. and subsequently tested for the photocatalytic reduction of carbon dioxide using triethylamine as a sacrificial donor and water as a reaction medium. The developed photocatalyst exhibited a significantly higher catalytic activity to give a methanol yield of 2570.78 μmol per g cat after 48 h.

Photocatalytic reduction of CO_2 to valuable chemicals such as methanol offers a promising way for clean, low cost and environmentally friendly production of fuels using solar energy.[1] Over the past few decades, enormous efforts have been devoted to the research of TiO_2 materials, which have been established as promising photocatalysts due to their low cost, low toxicity and versatility in terms of wide spread applications in various fields ranging from photovoltaics and photocatalysis to photo-/electrochromics and sensors.[2,3] In spite of these virtues, TiO_2 has some major drawbacks including absorption of only a small fraction (<5%) in the UV region of the solar spectrum and no absorption in the visible region. In addition, when TiO_2 catalysts are exposed to UV light, electrons in the uppermost valence band will jump to the conduction band and create photogenerated electrons and holes in the conduction and valence band, respectively. These electron–hole pairs on migration to the semiconductor surface interact with the adsorbed reactant, leading to the reduction of carbon dioxide to high value products.[4] However, in most instances, electrons and holes simply recombine and quench before reaching the catalyst surface, which is unfavourable for a photocatalytic reaction. Thus, extensive efforts are being pursued to modify the photo-physical properties of the TiO_2 photocatalyst for enhancing the charge separation efficiency that would result in a lower recombination rate. One of the elegant approaches for the modification of titanium dioxide is the surface sensitization or functionalization with metal complexes. These immobilized metal complexes can harvest visible light and inject photogenerated electrons into the conduction band of the titania.[5,6] Furthermore, efficient recovery of these nano-sized TiO_2 materials is still a challenge, which limits their widespread application. Magnetic separation provides a very convenient approach for the recovery and recycling of the nanoparticles/composites by applying external magnetic fields. Recently, a variety of magnetic supports (such as magnetite, barium ferrite, SiO_2@Fe_3O_4 particles and so on) have been employed as alternative catalyst supports for immobilizing TiO_2. These magnetic photocatalysts show not only an excellent photocatalytic activity but also an efficient magnetic recovery.[7,8] On the other hand, chemical functionalization or surface sensitization by using metal complexes especially phthalocyanine complexes, which are inexpensive, highly stable and can strongly absorb visible light will be a preferred approach for developing an efficient visible light active photocatalyst for the reduction of carbon dioxide to high value products such as methane and methanol. In addition, facile recovery and efficient recycling of the photocatalyst will make the process more viable from both environmental and economical viewpoints.[9]

Hence the major objective of the present work was to prepare a visible light active titania based nanocomposite photocatalyst with additional ferromagnetic properties for facile recovery and reuse. The objective was achieved *via* chemical attachment of tetrasulfonated cobalt phthalocyanine (CoPcS) to the TiO_2@SiO_2@Fe_3O_4 nanocomposite by using 3-aminopropyl-trimethoxysilane (APTS) as a linker. Sub-

[a]*Chemical Sciences Division, CSIR-Indian Institute of Petroleum, Mohkampur, Dehradun-248005, India. E-mail: suman@iip.res.in; Fax: +91-135-2660202; Tel: +91-135-2525788 (O)*
[b]*Analytical Sciences Division, CSIR-Indian Institute of Petroleum, Mohkampur, Dehradun-248005, India*

†Electronic supplementary information (ESI) available. See DOI: 10.1039/c4dt02461c

sequently, the Co-PcS functionalized nanocomposites were treated with $Ru(bpy)_2phen\text{-}NH_2$ to give magnetically separable Ru-CoPc@TiO_2@SiO_2@Fe_3O_4. The developed photocatalyst was found to be highly efficient visible light active, easily recoverable using an external magnet and recyclable for the reduction of carbon dioxide to methanol using water as a source of protons and triethylamine as a sacrificial donor. Importantly, the coating of Fe_3O_4 with a SiO_2 layer protected the nanomagnetite surface from oxygen and provided an improved stability towards oxidation.[10] Furthermore, the coating of SiO_2 provided plenty of –OH groups for efficient and stable loading of TiO_2 on the surface. Furthermore, the layer of SiO_2 between Fe_3O_4 and TiO_2 acted as an insulator which inhibits the recombination of photogenerated electrons and holes at the surface of the magnetic nanoparticles. After the screening of homogeneous Ru-CoPcS, $Ru(bpy)_2phen\text{-}NH_2$, CoPc-$(SO_2NH_2)_4$ and different combinations of heterogeneous catalysts such as CoPc@TiO_2@SiO_2@Fe_3O_4 and Ru@TiO_2@SiO_2@Fe_3O_4 and Ru-CoPc@TiO_2@SiO_2@Fe_3O_4, it was concluded that the particular formulation of Ru-CoPc@TiO_2@SiO_2@Fe_3O_4 provided efficient electron transfer to activate and reduce CO_2 to methanol under visible light.

Synthesis and characterization of the catalyst

During the present study, magnetically separable TiO_2@SiO_2@Fe_3O_4 **1** support was prepared by following the procedure as given in the Experimental section. The prepared material was found to be mesoporous as the mean pore diameter (7.5811 nm) was found to be between 2 and 50 nm.[11] The BET surface area and the total pore volume of the material were found to be 58.01 $m^2\ g^{-1}$ and 0.1099 $cm^3\ g^{-1}$ respectively (Fig. S1†). The surface of the magnetic composite **1** was then functionalized by using 3-aminopropyl trimethoxysilane (APTES) and subsequently treated with Ru-CoPcS complexes as shown in Scheme 1

The crystallinity and structure of as-prepared Fe_3O_4, TiO_2@SiO_2@Fe_3O_4 **1** and Ru-CoPc@TiO_2@SiO_2@Fe_3O_4 **6** were confirmed by XRD. As shown in Fig. 1, the peak position and relative intensity of Fe_3O_4 (Fig. 1a) matches well with standard powder diffraction data (JCPDS no. 74-2402), indicating the phase purity of Fe_3O_4. Well-resolved diffraction peaks reveal good crystallinity of **1** and **6** (Fig. 1b and c). In addition to all diffraction peaks of Fe_3O_4, there are other four diffraction peaks appearing at 2θ = 25.3°, 37.8°, 47.3°, and 54.21° which correspond to (101), (112), (200), and (211) planes of anatase TiO_2 (JCPDS no. 21-1272), respectively. The reduction of Fe_3O_4 peaks also confirmed the successful coating of TiO_2 to SiO_2@Fe_3O_4 composite. The XRD patterns of **6** (Fig. 1c) revealed the characteristic peaks of Ru-CoPc complex units (Fig. 1d), indicating that the crystallinity and morphology of the catalyst were preserved during immobilization. Importantly, the diffractogram of the samples (Fig. 1c) clearly indicated the signals of Ru/CoPc complex (Fig. 1d), confirming the higher loading of the complex to the photocatalyst support.

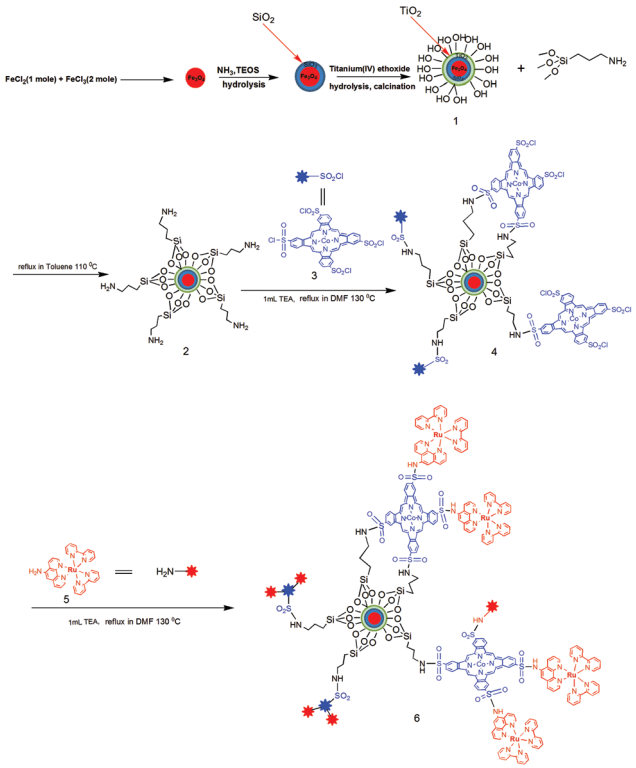

Scheme 1 Synthesis of photocatalyst **6**.

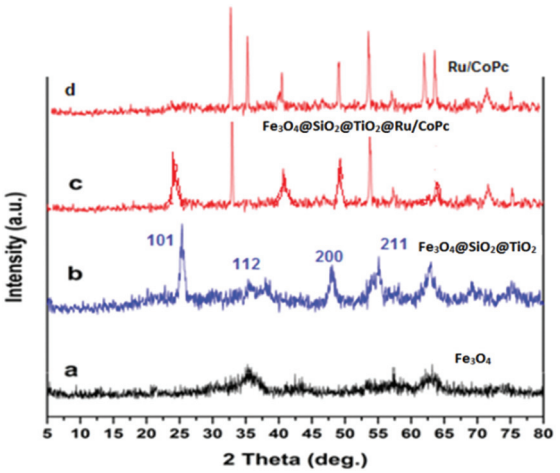

Fig. 1 XRD of (a) Fe_3O_4; (b) TiO_2@SiO_2@Fe_3O_4 **1**; (c) Ru-CoPc-TiO_2@SiO_2@Fe_3O_4 **6**; and (d) Ru-CoPc complex.

The morphologies of the synthesized samples were revealed by SEM (Fig. 2) and TEM (Fig. 3). The Fe_3O_4 crystallites are ultrafine and connected tightly together to form spheres with the particle size 300–500 nm (Fig. 2a). The egg-like structures of SiO_2@Fe_3O_4 microspheres with a diameter of 1–2 μm are shown in Fig. 2b. This indicated the successful coating of the SiO_2 onto the Fe_3O_4 nanoparticles. FE-SEM images of the TiO_2@SiO_2@Fe_3O_4 **1** and Ru-CoPc@TiO_2@SiO_2@Fe_3O_4 **6**

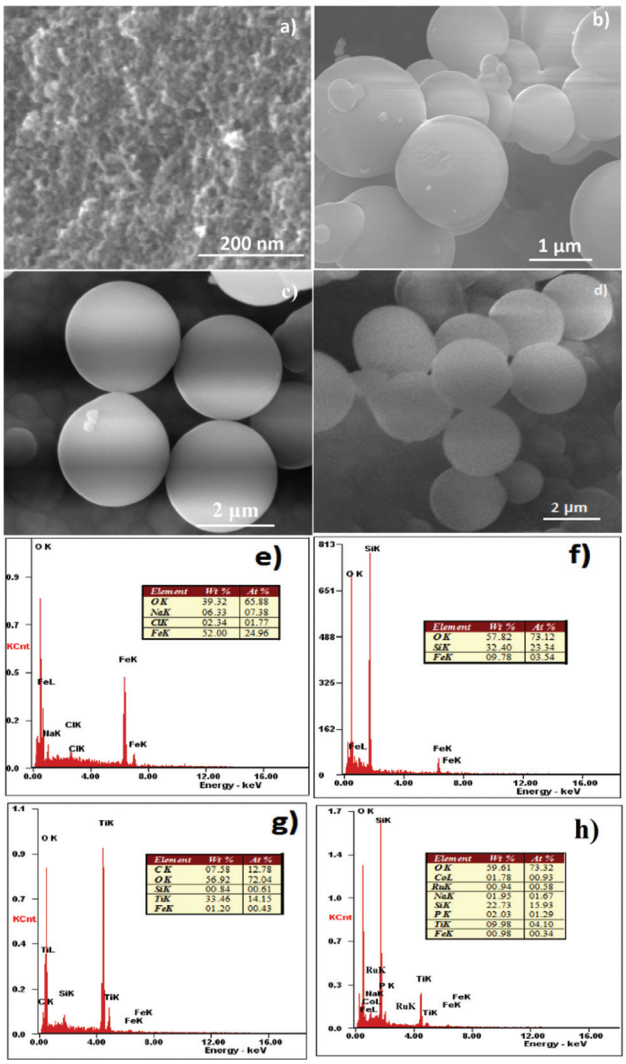

Fig. 2 FESEM images of (a) Fe_3O_4; (b) SiO_2@Fe_3O_4; (c) TiO_2@SiO_2@Fe_3O_4 **1**; (d) Ru-CoPc@TiO_2@SiO_2@Fe_3O_4 **6**; (e) EDX of **1**; (f) EDX of SiO_2@Fe_3O_4; (g) EDX of TiO_2@SiO_2@Fe_3O_4; and (h) EDX of **6**.

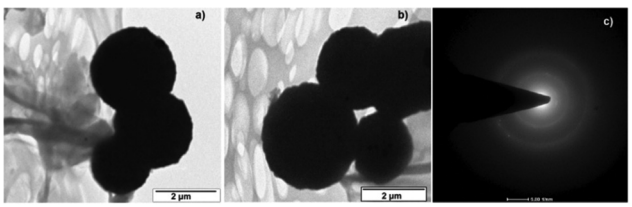

Fig. 3 TEM image: (a, b) Ru-CoPc@TiO_2@SiO_2@Fe_3O_4 **6**; (c) SAED pattern of **6**.

composites are shown in Fig. 2c and d respectively. As shown in Fig. 2c, a large number of SiO_2@Fe_3O_4 nanospheres are encapsulated in the core of TiO_2 shell, forming the egg-like structure, which provides a better surface for the immobilization of the Ru/CoPc complex. The as-synthesized nanocomposites **1** were composed completely of Fe, O, Si, and Ti as shown in Fig. 2e. Incessant reduction of iron content after coating of SiO_2 and TiO_2 revealed that the iron nanoparticles were successfully coated. EDX analysis of **6** (Fig. 2h) showed the presence of Fe, Si, Ti, O, Ru and Co elements.

Further we used TEM to examine the structure and morphology of **6** (Fig. 3). It is clearly indicated that particles in catalyst **6** retain a spherical morphology, non-aggregation, and a rough surface at all TiO_2 contents (Fig. 3a). Furthermore, Fig. 3b indicates the uneven distribution of the Ru/CoPc complex molecules to the nanocomposite support. Furthermore, rings in diffraction pattern in selected area electron diffraction showed that the material was polycrystalline in nature, suggesting that the crystallization of TiO_2 occurred during calcinations.

FT-IR was used to characterize the composition and structure of the **1** and Ru-CoPc@TiO_2@SiO_2@Fe_3O_4 composites **6** (Fig. 4). The FTIR spectrum of **1** (Fig. 4c) shows characteristic peaks at 570 cm^{-1} corresponding to the vibration of the Fe–O functional group,[12] at 800 cm^{-1} corresponding to the symmetric vibration of Si–O–Si; and a broad peak at 621 cm^{-1} corresponding to the Ti–O–Ti.[13] The peaks at 1644 and 3434 cm^{-1} can be attributed to absorption by water and hydroxyl groups.[14] This surface hydroxylation is advantageous for the photocatalytic activity of TiO_2@SiO_2@Fe_3O_4 microspheres because it provides a higher capacity for oxygen adsorption.[15] FTIR spectra of CoPc-Ru@TiO_2@SiO_2@Fe_3O_4 **6** showed the additional peaks which are related to the phthalocyanine and bipyridyl functional groups as shown in Fig. 4d. As shown in Fig. 4d, all of the vibrational bands of the Ru complex and the CoPc are not found in the composite, which is probably due to the partial degradation upon immobilization.

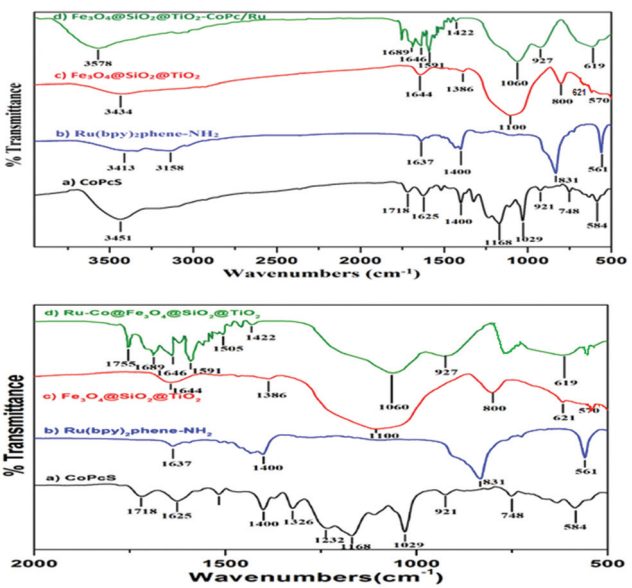

Fig. 4 FTIR spectra of: (a) CoPcS; (b) Ru(bpy)$_2$phene-NH_2; (c) TiO_2@SiO_2@Fe_3O_4 **1**; (d) Ru-CoPc@TiO_2@SiO_2@Fe_3O_4 **6** and expanded region 500 cm^{-1} to 2000 cm^{-1}.

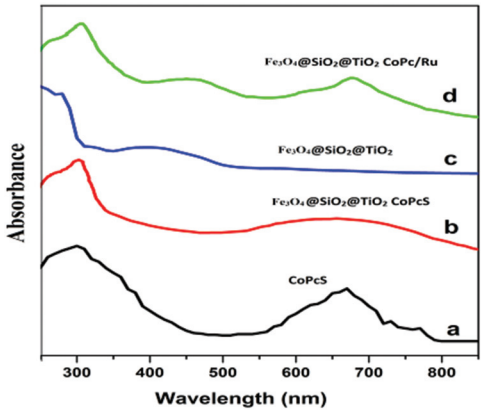

Fig. 5 UV-Vis spectra of: (a) CoPcS; (b) CoPc@TiO_2@SiO_2@Fe_3O_4; (c) TiO_2@SiO_2@Fe_3O_4 and (d) Ru-CoPc@TiO_2@SiO_2@Fe_3O_4 **6**.

The UV–vis absorption spectra of the as-synthesized samples are shown in Fig. 5. Absorption spectra of CoPcS and Ru(bpy)$_2$phene-NH_2 complexes were taken in acetonitrile, whereas absorption of TiO_2@SiO_2@Fe_3O_4 and Ru-CoPc-TiO_2@SiO_2@Fe_3O_4 **6** were studied in the solid state. UV/Vis absorption spectra of CoPcS shows two characteristic absorption bands *e.g.* at 300 nm (Soret band) and 670 nm (Q band)[16,17] (Fig. 5a). It is observed that the TiO_2@SiO_2@Fe_3O_4 and Ru-CoPc@TiO_2@SiO_2@Fe_3O_4 nanocomposites exhibit remarkable absorbance in the visible region beyond 400 nm. Absorption spectrum of **6** shows the characteristic Soret band of CoPc near 350 nm, indicating the successful attachment of the complexes to the support. The absorption band wavelength shifted to the visible range when Ru-CoPcS complex units were immobilized on the surface of TiO_2@SiO_2@Fe_3O_4 (Fig. 5d).

The thermal stability of the catalyst was determined by thermogravimetric analysis. The DT-TGA curve of the catalyst **6** indicated constant weight loss over the temperature range of 100–800 with a slight variance in its slope at two points (Fig. 6). The first degradation was observed at 325 °C, probably due to the breakdown of Ru complex unit. The second weight loss was observed at 550 °C, which might be attributed to the degradation of phthalocyanine unit.

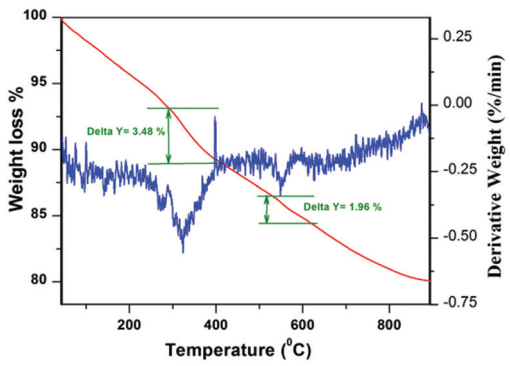

Fig. 6 DT-TGA curve of Ru-CoPc@TiO_2@SiO_2@Fe_3O_4 **6**.

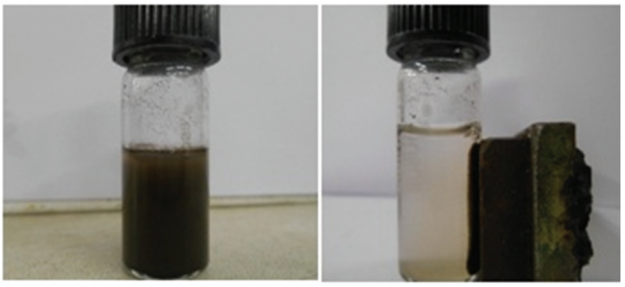

Fig. 7 Magnetic separation of the catalyst **6** using an external magnetic effect.

Magnetic separation provides a very convenient approach for removing and recycling magnetic catalysts. The magnetism of the catalyst **6** was tested in water by placing a magnet near the glass bottle (Fig. 7). The dark brown particles were attracted toward the magnet with time and completely separated after 5 min, leaving a clear solution. So the as-prepared catalyst can be easily recovered by the influence of an external magnet after the photocatalytic process.

The photocatalytic reduction of CO_2

First of all we performed a blank experiment for the photocatalytic reduction of CO_2 by using triethylamine as a sacrificial donor and water as a reaction medium. The reaction did not produce any organic product (Fig. 8). Next, we checked the catalytic activity of the homogeneous Ru-CoPcS, Ru(bpy)$_2$phen-NH_2 and CoPc$(SO_2NH_2)_4$ under identical experimental conditions (Fig. 8). The reactions were found to be very slow and gave only a trace yield of methanol as determined by GC. Further we tested the activity of synthesized heterogeneous photocatalysts, *i.e.* Ru/CoPc@$Fe_3O_4TiO_2$@SiO_2 and Ru-CoPc@SiO_2@Fe_3O_4. The results of these experiments are given in

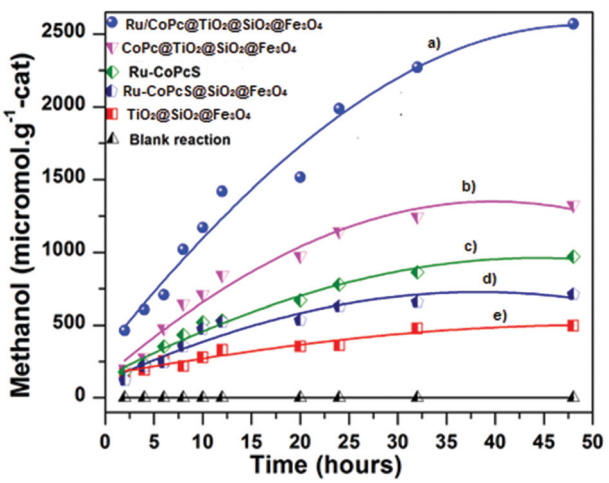

Fig. 8 Methanol yield using (a) Ru/CoPc@TiO_2@SiO_2@Fe_3O_4 **6**; (b) CoPc@TiO_2@SiO_2@Fe_3O_4 **6**; (c) Ru-CoPcS; (d) Ru-CoPcS@SiO_2@Fe_3O_4; (e) TiO_2@SiO_2@Fe_3O_4; and (f) blank run.

Fig. 8. Methanol yield was used to evaluate the performance of the catalysts as it was obtained as the major reduction product. Other products might have formed but in small quantities and therefore could not be detected. According to the procedure described in the Experimental section, the methanol (MeOH) formation rate, R_{MeOH} (μmol per g cat) was calculated and plotted in Fig. 8 as a function of reaction. Among the various catalysts studied, the catalyst **6** was found to be the best and provided the highest yield of methanol under similar reaction conditions. After illumination for 48 h in visible light in the presence of triethylamine as a sacrificial donor, the yield of methanol was found to be 2570.18, 1324.60 and 496.72 μmol g^{-1}cat by using Ru-CoPc@TiO_2@SiO_2/Fe_3O_4, CoPc@TiO_2@SiO_2@Fe_3O_4 and Ru-CoPc@SiO_2/Fe_3O_4 as catalysts respectively. Furthermore, the presence of Ru-complex in nanocomposite **6** exhibited a significant enhancement in the yield of methanol. The superior catalytic activity due to the presence of Ru and Co-complexes in catalyst **6** can be explained as follows: the ruthenium's singlet state because of its higher energy and shorter lifetime of the excited state (~0.385 to 0.421 μs) than CoPc (~170 to 245 μs), rapidly transfers electrons to the conduction band of CoPc. On the other hand, the excited state (S1) of CoPc has a higher energy and a longer lifetime in comparison with the conduction band of TiO_2, so it efficiently transfers electrons to the conduction band of TiO_2, which is subsequently used for the reduction of carbon dioxide.[17–21] The possible mechanistic pathway for the reaction is shown in Scheme 2.

The conversion of CO_2 to methanol was confirmed using GC-FID, and ^{1}H NMR analysis (Fig. S4†). Blank experiments, in the absence of the photocatalyst as well as in the dark reaction, showed that there was no organic product found for long periods of CO_2 photoreduction. Further additional blank run having all identical conditions (catalyst, solvent, irradiation, and reaction time) except using N_2 instead of CO_2 did not give any product, confirming that methanol was formed due to the photoreduction of CO_2.

To confirm the formation of methanol from CO_2, isotopic labelling experiment was performed by using $^{13}CO_2$ instead of $^{12}CO_2$. After photoreaction with $^{13}CO_2$, the generated methanol gave a peak at *m*/*z* value 33 in GC-MS (Fig. S6†), confirming the origin of methanol from CO_2 photoreduction.

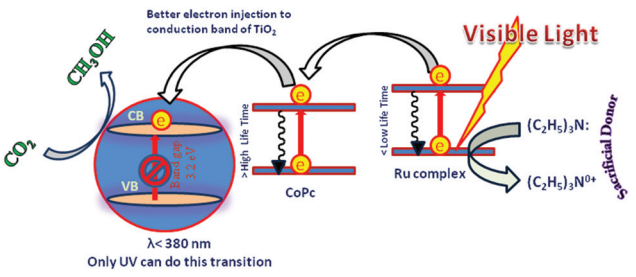

Scheme 2 Possible mechanism for the photoreduction of CO_2 to methanol.

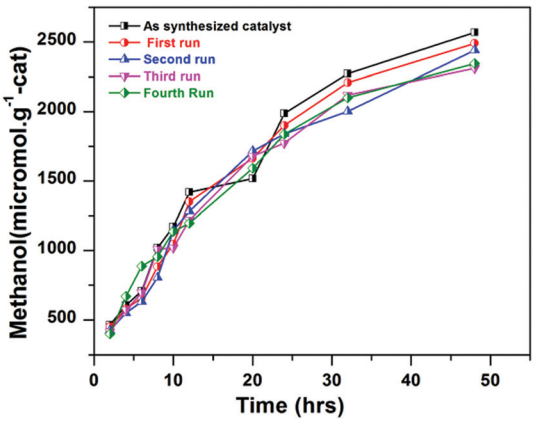

Fig. 9 Recycling of the catalyst.

After completion of the reaction, the catalyst was easily recovered by using an external magnet, washed with deionized water and subsequently used for recycling experiment. The recovered catalyst was used for the subsequent four runs under identical experimental conditions. The results of these recycling experiments are summarized in Fig. 9. Almost similar yield of methanol in all cases confirmed the efficient recycling and stability of the catalyst. Furthermore, ICP-AES analysis of the recovered catalyst after four recycling runs gave (Co-0.98 wt%; Ru-0.94 wt%) suggested that the negligible leaching had occurred during the reaction.

Conclusions

In conclusion, we have developed novel and highly efficient magnetic TiO_2@SiO_2@Fe_3O_4 nanocomposites chemically attached with CoPc and Ru-complexes for the photoreduction of CO_2 to methanol. The presence of ruthenium bipyridyl moieties exhibited remarkable enhancement in the catalytic activity of **6** and yielded methanol in 2570.78 μmol per g cat under visible light irradiation after 48 h. These conversion rates are much higher than that of other formulated heterogeneous catalysts such as TiO_2@SiO_2@Fe_3O_4 and CoPc-TiO_2@SiO_2@Fe_3O_4. Furthermore, covalent attachment of the complexes to the composite support prevents leaching of active metal species during the reaction. Moreover, the magnetic catalyst could easily be separated by using an external magnet effect, which provides an efficient and facile recovery of the catalyst with minimal loss. We believe that the developed magnetic Ru-CoPc@TiO_2@SiO_2@Fe_3O_4 composite catalyst may open new avenues for various potential applications in photo-catalysis.

Experimental section

UV-visible absorption spectra were collected with a Perkin Elmer lambda-19 UV-VIS-NIR spectrophotometer using a 10 mm quartz cell. Fourier Transform Infrared Spectroscopy (FT-IR) was conducted using a Perkin-Elmer spectrum RX-1 IR

spectrophotometer. High resolution transmission electron microscopy (HR-TEM) of $Fe_3O4@SiO_2@TiO_2$ Co/Pc composite was executed using Phillips CM 200 operating at an acceleration voltage of 200 kV. Scanning electron microscopy (SEM) and Energy dispersive X-ray spectroscopy (EDX) were performed using a Jeol Model JSM-6340F. For FE-SEM analysis aqueous dispersions of Fe_3O_4 based support and Ru-CoPc@$Fe_3O_4@SiO_2/TiO_2$ composite were deposited on glass slides, while very dilute aqueous suspensions were deposited on carbon coated copper grids for HR-TEM analysis. X-ray powder diffraction (XRD) analyses were performed on a Bruker D8 Advance diffractometer at 40 kV and 40 mA with Cu K_α radiation (λ = 0.15418 nm). Thermogravimetric analyses (TGA) of these samples were carried out using a thermal analyzer TA-SDT Q-600. All samples were analyzed in the temperature range of 40 to 800 °C at a heating rate of 10 °C min^{-1} under nitrogen flow. The porous properties of $Fe_3O_4@SiO_2/TiO_2$ support were examined using N_2 adsorption–desorption isotherms at 77 K and the related data (surface area, S_{BET}; pore volume, V_P; Micromeritics ASAP2010) were calculated. The conversions and selectivity of the products were determined by GC-FID (Varian CP-3800). ^{1}H-NMR spectra of the Ru(bpy)$_2$phene-NH_2 and photoreaction products were performed at 500 MHz by using a Bruker Avance-II 500 MHz instrument in DMSO-d_6. ICP-AES analysis was carried out using an inductively coupled plasma atomic emission spectrometer (ICP-AES, DRE, PS-3000UV, Leeman Labs, USA). (Sample for ICP-AES was prepared by leaching out 0.01 g of sample with conc. HNO_3 heated for 30 min and then volume of the solution was made up to 10 mL).

Synthesis of iron nanoparticles[22]

Iron nanoparticles were synthesized by mixing ferrous chloride and ferric chloride solution in alkaline aqueous medium by following a literature procedure. In a typical experiment, 5.2 g of $FeCl_3$ and 2.0 g of $FeCl_2$ were dissolved in 25 mL deoxygenated water that contains 0.85 mL of 12.1 N HCl solution. The resulting solution was then added dropwise to 1.5 M NaOH (250 mL) with vigorous stirring. The isolated iron nanoparticles were separated by using an external magnet and centrifugation. The isolated product was thoroughly washed with water and finally treated with 0.01 M HCl (500 mL). The product was centrifuged and dried for further use.

Preparation of $SiO_2@Fe_3O_4$ nanoparticles[23,24]

The Fe_3O_4 nanoparticles (2 g) were ultrasonicated for 1 h to uniformly disperse in a mixture of water (5 mL) and ethanol (45 mL). Concentrated ammonium hydroxide (10 mL) was diluted with the above solution and tetraethylorthosilicate (TEOS; 15 mL) was quickly added under vigorous stirring. The solution was allowed to stir for 5 h. The product was collected by centrifugation and washed with anhydrous ethanol three times and dried.

Synthesis of nanocomposite[25] 1

Titanium(IV) ethoxide (2 mL) was dissolved in 100 mL ethanol and stirred for five minutes. The resulting $SiO_2@Fe_3O_4$ nanocomposites (5 g) were re-dispersed in anhydrous ethanol (50 mL) by using sonication. Subsequently, a solution as prepared by dissolving titanium(IV) ethoxide (2 mL) in ethanol (100 mL) was introduced dropwise to the above mentioned suspension of $SiO_2@Fe_3O_4$ nanocomposites, followed by heating the solution at about 70 °C. The whole process was performed under vigorous stirring. After 3 h, the resulting dark brown precipitates were separated using an external magnet and filtration. The resulting product was washed with deionized water and ethanol five times and calcined at 500 °C for 3 h under a nitrogen atmosphere.

Functionalization of $TiO_2@SiO_2@Fe_3O_4$ by 3-aminopropyl trimethoxysilane[26] 2

$TiO_2@SiO_2@Fe_3O_4$ nanocomposites (5 g) were taken in toluene (50 mL) and 3-aminopropyl trimethoxysilane (4 mL) was added. The resulting mixture was sonicated for five minutes and then refluxed for 24 h. The isolated product was collected by filtration and washed with ethanol and dried under vacuum.

Immobilization of CoPcS[27] complexes to chemically functionalized $TiO_2@SiO_2@Fe_3O_4$ support 4

3-Aminopropyl silylated nanocomposite **2** was taken in DMF (20 mL) and cobalt phthalocyaninetetrasulfonyl chloride **3** (0.5 g), triethylamine (1 mL) were added. The resulting mixture was refluxed for 24 h under a nitrogen atmosphere. The product CoPc-$TiO_2@SiO_2@Fe_3O_4$ nanocomposite **4** was collected by filtration. The isolated material was thoroughly washed with DMF until the color of the filtrate disappeared. DMF was used for preventing the hydrolysis of SO_2Cl groups back to SO_3OH groups.

Synthesis of $Ru(bpy)_2Cl_2{\cdot}2H_2O$[28]

2-2′Bipyridine (2.34 g, 15 mmol), $RuCl_3{\cdot}3H_2O$ (1.95 g, 7.45 mmol) and lithium chloride (2.1 g, 50 mmol) were dissolved in DMF (20 mL) and refluxed for 8 h. The reaction mixture was allowed to cool to room temperature, followed by the addition of acetone (125 mL) slowly. The resulting mixture was refrigerated at 0 °C for 12 h. The isolated product was filtered using a membrane filter under vacuum. The product was washed several times with deionized water and diethyl ether to remove the impurities of unreacted substrates. Finally the product was dried under vacuum and used for the subsequent step. The synthesized complex was confirmed by ^{1}H NMR spectroscopy (Fig. S3†).

Synthesis of $[Ru(bpy)_2phene\text{-}NH_2](PF_6)_2$[29,30] 5

The resulting $Ru(bpy)_2Cl_2{\cdot}2H_2O$ (1.453 g, 3 mmol) and 1,10 phenanthroline 5-amine (0.600 g, 3 mmol) in ethanol was refluxed for 15 hours under a nitrogen atmosphere. The mixture was filtered through a membrane filter paper to remove the undissolved reactants. Then the saturated solution of NH_4PF_6 was added to the filtrate followed by placing the resulting mixture in the refrigerator for 12 h. The isolated

precipitate was collected by filtration under vacuum, washed with cold water, diethyl ether and dried under vacuum.

Synthesis of the Ru-CoPc@TiO_2@SiO_2@Fe_3O_4 nanocomposites 6

The resulting CoPcS immobilized TiO2@SiO2@Fe3O4 nanocomposites were taken in DMF and treated with $Ru(bpy)_2$-phene-NH_2 (0.5 g). The resulting mixture was refluxed in the dark for 24 h under a nitrogen atmosphere. The resulting nanocomposite 6 was isolated with an external magnet and washed with DMF, ethanol until the filtrate became colorless. Finally the resulting material was dried under vacuum. The analytical values of 6 were found to be C 4.916%; H 1.696%; N 1.305%. The loading of metal complexes in 6 was estimated by ICP-AES analysis and weight% of Co and Ru were found to be 1.26% and 1.17% respectively.

Photocatalytic reduction of CO_2

Photocatalytic experiment was performed in a 100 mL borosil cylindrical vessel of 5 cm diameter. Photoirradiation was carried out under visible light by using 20 watt white cold LED flood light (Model no.-HP-FL-20W-F-Hope LED Opto-Electric Co. Ltd, $\lambda > 400$ nm). The whole spectrum of LED light was used for illumination purpose. The intensity of the light at the middle of vessel was found to be 78 W m^{-2} as determined using an intensity meter. The vessel was charged initially with water (40 mL) and triethylamine (10 mL) and then the solution was degassed by continuous purging of nitrogen for 15 min. Then CO_2 was bubbled through the solution for at least 30 min to saturate the solution. As synthesized photocatalyst **6** (100 mg) was added to the above solution and the vessel was closed tightly during the reaction and stirred vigorously to prevent the sedimentation of the catalyst. Samples were collected after every 2 h intervals with the help of a long needle and the catalyst was removed using a syringe filter (2 nm PTFE, 13 mm diameter). Quantitative determination was done by using gas chromatography FID (Varian CP-3800, having 30 m long Stabilwax® w/Integra-Guard® column) at flow rate 0.5 mL min^{-1}, injector temp., 250 °C, and FID detector temp., 275 °C. A calibration curve was prepared for quantification and confirmation of linear response of the GC-FID system, Fig. S2.†

Blank reactions were conducted to ensure that methanol production was due to the photo-reduction of CO_2, and to eliminate surrounding interference. One blank reaction was carried out under visible light without the catalyst, and another was performed in the dark in the presence of catalyst under identical experimental conditions. An additional blank test was vis-illuminated with the catalyst filling N_2 rather than CO_2. No product was detected in the above three blank tests.

Acknowledgements

We kindly acknowledge Director, CSIR-IIP for his kind permission to publish these results. PK is thankful to CSIR, New Delhi for providing research fellowship under the Emeritus Scientist Scheme. Analytical division of the Institute is kindly acknowledged for providing support in analysis of samples.

Notes and references

1 G. A. Olah, *Angew. Chem., Int. Ed.*, 2013, **52**, 104–107.
2 A. Fujishima and K. Honda, *Nature*, 1972, **238**, 37–38.
3 A. J. Morris, G. J. Meyer and E. Fujita, *Acc. Chem. Res.*, 2009, **42**, 1983–1994.
4 M. Ni, M. K. H. Leung, D. Y. C. Leung and K. Sumathy, *Renewable Sustainable Energy Rev.*, 2007, **11**, 401–425.
5 D. Dvoranová, V. Brezová and M. A. Malati, *Appl. Catal., B*, 2002, **37**, 91–105.
6 X. Chen and S. S. Mao, *Chem. Rev.*, 2007, **107**, 2891–2959.
7 C.-J. Li, J.-N. Wang, B. Wang, J. R. Gong and Z. Lin, *Mater. Res. Bull.*, 2012, **47**, 333–337.
8 R. B. N. Baig and R. S. Varma, *Chem. Commun.*, 2013, **49**, 752.
9 Z. Guo, C. Shao, M. Zhang, J. Mu, Z. Zhang, P. Zhang, B. Chen and Y. Liu, *J. Mater. Chem.*, 2011, **21**, 12083.
10 (*a*) J. Huang, C. Liu, H. Xiao, J. Wang, D. Jiang and E. Gu, *Int. J. Nanomed.*, 2007, **2**, 775; (*b*) J. G. Guan, J. Haung, S. L. Zhao and R. Z. Huan, *Int. J. Mod. Phys. B*, 2001, **15**, 599.
11 I.UP.AC. Recommendations, *Pure Appl. Chem.*, 1994, **66**, 1739.
12 J. Kim, J. Kim and M. Lee, *Surf. Coat. Technol.*, 2010, **205**, 372–376.
13 A. Zielinska, E. Kowalska, J. W. Sobczak, I. Lacka, M. Gazda, B. Ohtani, J. Hupka and A. Zaleska, *Sep. Purif. Technol.*, 2010, **72**, 309–318.
14 X. X. Yu, S. W. Liu and J. G. Yu, *Appl. Catal., B*, 2011, **104**, 12–20.
15 J. Wang, X. Liu, R. Li, P. Qiao, L. Xiao and J. Fan, *Catal. Commun.*, 2012, **19**, 96–99.
16 *Phthalocyanines, Properties and Applications*, ed. C. C. Leznoff and A. B. P. Lever, VCH, Cambridge, 1989, vol. 1–4.
17 B. D. Berezin, *Synthesis and Reactivity in Inorganic and Metal-Organic Chemistry*, John Wiley & Sons, 1981.
18 Y. Yu, M. Zhou and H. Cui, *J. Mater. Chem.*, 2011, **21**, 12622–12625.
19 R. Hinogami, Y. Nakamura, S. Yae and Y. Nakato, *J. Phys. Chem. B*, 1998, **102**, 974–980.
20 J. R. Darwent, P. Douglas, A. Harriman, G. Porter and M. C. Richoux, *Coord. Chem. Rev.*, 1982, **44**, 83–126.
21 C. V. Kumar, J. K. Barton and N. J. Turro, *J. Am. Chem. Soc.*, 1985, **107**, 5518–5523.
22 E. M. Kober and T. J. Meyer, *Inorg. Chem.*, 1982, **21**, 3967–3977.
23 Y. S. Kang, S. Risbud, J. F. Rabolt and P. Stroeve, *Chem. Mater.*, 1996, **8**, 2209–2211.
24 Z. Wang, L. Shen and S. Zhu, *Int. J. Photoenergy*, 2012, **2012**, 1–6.

25 A. Rezaeifard, M. Jafarpour, A. Naeimi and R. Haddad, *Green Chem.*, 2012, **14**, 3386.
26 B. Karimi and E. Farhangi, *Chem. – Eur. J.*, 2011, **17**, 6056–6060.
27 G. Das, B. Sain, S. Kumar, M. O. Garg and G. Murali Dhar, *Catal. Today*, 2009, **141**, 152–156.
28 B. P. Sullivan, D. J. Salmon and T. J. Meyer, *Inorg. Chem.*, 1978, **17**, 3334–3341.
29 M. Kobayashi, S. Masaoka and K. Sakai, *Molecules*, 2010, **15**, 4908–4923.
30 W. Haung and T. Ogawa, *Polyhedron*, 2006, **25**, 1379–1385.